MPC Algorithm With Reduced Computational Burden and Fixed Switching Spectrum for a Multilevel Inverter in a Photovoltaic System

JOSE J. SILVA [ID]**[1], (Member, IEEE), JOSE R. ESPINOZA** [ID]**[1], (Senior Member, IEEE),**
JAIME A. ROHTEN [ID]**[2], (Member, IEEE), ESTEBAN S. PULIDO** [ID]**[3], (Student Member, IEEE), FELIPE**
A. VILLARROEL [ID]**[1], MIGUEL A. TORRES** [ID]**[4], (Member, IEEE), AND MAURICIO A. REYES** [ID]**[1]**
[1]Department of Electrical Engineering, Universidad de Concepción, Concepción 4070386, Chile
[2]Department of Electrical and Electronic Engineering, Universidad del Bío-Bío, Concepción 4051381, Chile
[3]Department of Electrical Engineering, Universidad Técnica Federico Santa María, Valparaíso 2340000, Chile
[4]Intituto de Ciencias de la Ingeniería, Universidad de O'Higgins, Rancagua 2841158, Chile

Corresponding author: Jaime A. Rohten (jrohten@ubiobio.cl)

ABSTRACT Renewable energy has gained significant attention of researchers in the last years, mainly due to the importance of using unlimited energy sources to supply homes, industries, cities and countries. In this context, this document focuses on the solar injection by employing a neutral point clamped (NPC) topology together with utilization of a maximum power point tracking (MPPT) and space vector modulation (SVM) techniques. Model predictive control (MPC) is employed to manage the currents and track their references. The proposed algorithms do not employ a cost function to decide which voltage to apply resulting in a spread frequency spectrum, and instead, a concentrated SVM spectrum is imposed. Notwithstanding, the DC link capacitors voltage balance is ensured and the computational burden is notably reduced as compared to traditional Finite Set Model Predictive Control (FS-MPC). Nevertheless, the consistent results are a consequence of the critical analysis that shows the feasibility of the proposal and guarantees the good performance of the entire system in simulated and experimental platforms.

INDEX TERMS Predictive control, Solar power generation, AC-DC power converters, Fast MPC, Fixed switching spectrum MPC.

I. INTRODUCTION

Governments around the globe have been promoting the use of renewable and clean energies, being the most popular sources the solar and wind energy, and also promoting electric mobility as a part of the carbon dioxide emission reduction, [1]. Therefore, investigations that help to improve and make clean energies more efficient are of particular interest. The sun irradiance is a lifetime unlimited source that may be employed to supply the growing number of automatic devices used in this electric-dependent world. On this line, many researchers have been working towards improved renewable energy injection systems. The improvements refer to the

The associate editor coordinating the review of this manuscript and approving it for publication was Mauro Gaggero [ID].

control algorithms, the power topology and the whole system efficiency [2].

Solar irradiation can be harvested in all around the globe, although the intensity and temperature are different in every single place and also change during the day. Those two parameters -the irradiance and temperature- are critical in solar photovoltaic (PV) systems, because the harvested amount of energy depends directly of these two variables. To increase the efficiency of the photovoltaic systems, several MPPT algorithms have been proposed and the most used ones are perturb and observe (P&O) [3], incremental conductance (InC) [4] and measuring cells based (MCB) [5]. These MPPT algorithms have been implemented in (*i*) DC/DC converters [6], where the inverter DC link voltage is controlled and independent of the PV MPPT voltage, or (*ii*) directly on the
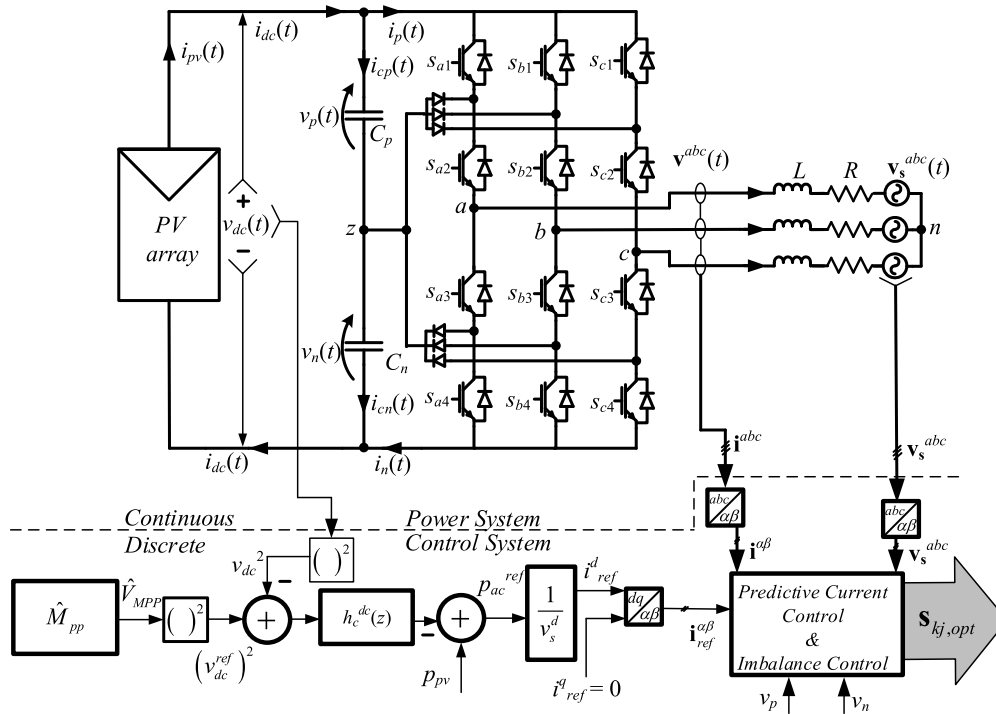
FIGURE 1. NPC Grid tie inverter using BPV Cells including controlf scheme.

inverters control strategy [7], where the DC link voltage is imposed by the MPPT, but the additional DC/DC stage is removed and therefore the total efficiency increases.

Nowadays, monofacial solar panels dominate the market [8]; however bifacial photovoltaic (BPV) technology has been shown to significantly increase the performance of photovoltaic modules [9] and is increasingly being considered in photovoltaic systems, due to their enhanced generation capability in terms of watts per area [10].

To be able to inject the power coming from the array of BPV cells, topologies such as the cascaded H-bridge (CHB) [11], active front end (AFE) [12], and neutral point clamped (NPC) [13] have been proposed, among others. The control algorithm is to be adapted for every topology, where the most common are: (*i*) linear control, such as proportional-resonant control, repetitive control and classic proportional-integral (PI) controllers, [14], (*ii*) nonlinear based control and nonlinear feedback linearization [15] and (*iii*) model predictive control, as finite-set MPC, and deadbeat control (DB), [12], [16], being MPC of particular interest in this work.

This work presents a control of a solar plant directly connected to the power grid, which uses a NPC multi-level inverter, where the proposed control strategy is a combined linear control and predictive control scheme with extended horizon and fixed switching frequency to obtain a low fluctuation of the neutral point (imbalance of the DC capacitors) and a low distortion in the AC currents. To operate the photovoltaic array at the maximum power point (MPP), a linear discrete PI controller is used to regulate the DC voltage

whose reference is generated by the MPPT algorithm. On the NPC AC side, to control the current $i^{abc}(t)$, a variation of the FS-MPC is used, named fast-finite-set MPC (FFS-MPC), whose reference is generated by the DC link voltage linear controller, including a unitary power factor (PF) reference. The FFS-MPC is easy to implement, since it becomes a modified version of the standard FS-MPC, and the computational burden is reduced, requiring no specific hardware.

In conventional MPC, a restricted model is minimized for a finite time horizon, whose minimization delivers the control output. Due to the rapid dynamics of electrical systems, a relatively high sampling frequency is generally required, which leaves little time available for the acquisition of the variables and the calculation of the optimization problem in real time. An alternative to the conventional MPC proposed in [17], which only has one cost function, is the finite set model predictive control that separates the cost functional in order to reduce the computing time [18]. In this algorithm, control variables are predicted for each valid switching state; then, a cost function is evaluated and, finally, the state that minimizes the cost function is applied throughout the sampling period. Thus, FS-MPC has become an interesting approach, thanks to its advantages, such as rapid dynamic response, simple inclusion of nonlinearities, restrictions, implementation in multi-objective control systems, etc.

In this work, the mathematical model associated with the various elements of the proposed scheme is obtained in the form of state variable equations. Next, a discrete approximation of the state equations in the time domain of the system

is deduced in order to develop and propose a discrete mixed control strategy. Then, the proposed control strategy is simulated and applied in a photovoltaic system in PSim. Finally, several experimental tests are carried out to validate the model and the proposed control algorithm and the key design guides are also provided. The most relevant conclusions of the work are also included.

II. MATHEMATICAL MODEL

A photovoltaic system connected directly to the network is presented in FIGURE 1. The scheme has a large array of bifacial photovoltaic modules (BPVs) and 2 capacitors (C_p, C_n) on the DC side of the multilevel inverter and a first order filter (R-L) connected to the simplified AC network (v_s). In the following, the mathematical model on the AC side, DC side of the converter, the three levels NPC converter, and the BPV array model are developed.

A. MODEL AT THE AC SIDE OF THE NPC

Applying the voltage Kirchhoff law on the AC side FIGURE 1, the following relationship is obtained:

$$\mathbf{v}^{abc}(t) = L\frac{d}{dt}\mathbf{i}^{abc}(t) + R\mathbf{i}^{abc}(t) + \mathbf{v}_s^{abc}(t) \quad (1)$$

where $\mathbf{v}^{abc}$ is the output voltage of the converter, $\mathbf{i}^{abc}$ is the injected current, and $\mathbf{v}_s^{abc}$ is the grid voltage.

Using the Clarke power invariant transformation and rewording, the model in $\alpha\beta$ axis is:

$$L\frac{d}{dt}\mathbf{i}^{\alpha\beta}(t) = \mathbf{v}^{\alpha\beta}(t) - R\mathbf{i}^{\alpha\beta}(t) - \mathbf{v}_s^{\alpha\beta}(t), \quad (2)$$

where the power invariant transformation is:

$$\mathbf{x}^{\alpha\beta} = \sqrt{\frac{2}{3}}\begin{bmatrix} 1 & -\frac{1}{2} & -\frac{1}{2} \\ 0 & \frac{\sqrt{3}}{2} & -\frac{\sqrt{3}}{2} \end{bmatrix}\mathbf{x}^{abc}. \quad (3)$$

B. MODEL AT THE AC SIDE OF THE NPC

The NPC inverter has 3 legs (one leg per phase, $k = \{a,b,c\}$) and each leg has 4 switches ($j = \{1, 2, 3, 4\}$), the combinations of these switches are limited (so as not to damage the equipment) and can only generate 3 possible states per phase. The states (γ^k) of each leg k

$$\gamma^k = \begin{cases} 1 & (S_{k1} = 1, S_{k2} = 1) \\ 0 & (S_{k1} = 0, S_{k2} = 1) \\ -1 & (S_{k1} = 0, S_{k2} = 0) \end{cases} \text{ and } \begin{matrix} S_{k3} = \bar{S}_{k1} \\ S_{k4} = \bar{S}_{k2} \end{matrix} \quad (4)$$

These three possible states per leg can generate 27 (3³) possible configurations, giving 19 possible output voltages to the AC side, FIGURE 2 (a), where
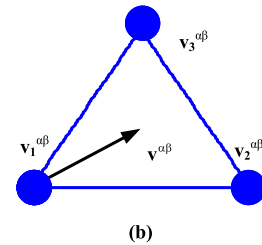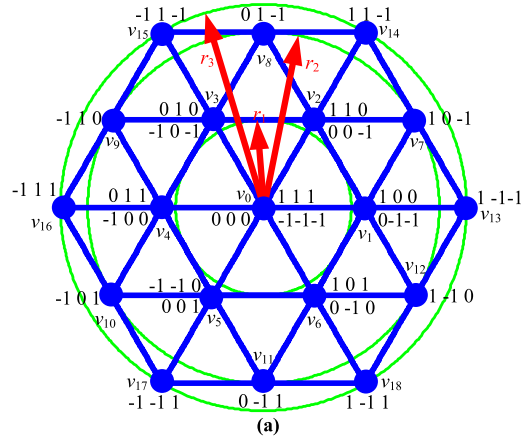

FIGURE 2. Valid States for the power converter (a) all 27 states, (b) highlighting the three nearest voltages for a given voltage $\mathbf{v}^{\alpha\beta}$.
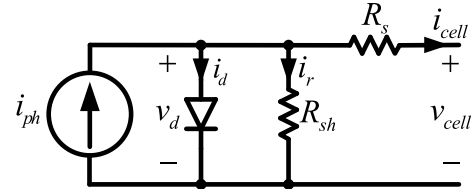

FIGURE 3. Equivalent electrical circuit of a BPV cell model.

$$\mathbf{v}_j^{\alpha\beta} = \begin{cases} 0 & , j = 0 \\ \frac{\sqrt{2}}{2}v_{dc}e^{(j-1)\frac{\pi}{3}} & , j = 1, .., 6 \\ \frac{1}{\sqrt{6}}v_{dc}e^{(j-7)\frac{\pi}{3}+\frac{\pi}{6}} & , j = 7, .., 12 \\ \sqrt{\frac{2}{3}}v_{dc}e^{(j-12)\frac{\pi}{3}} & , j = 13, .., 18 \end{cases} \quad (5)$$

The 19 possible normalized output voltages ($v_j, j = \{0, 1, \ldots, 18\}$), where $r_3 = \sqrt{2/3}$, which depend on the switching state of each section (γ^k) and therefore on the 27 possible states (ST). The voltage 0 can be generated by 3 possible states (-1, 0, 1), the short voltages (1, 2,..., 6) can be generated by 2 combinations each one and the medium (7,..., 12) and long voltages (13,..., 18) are generated only by one state.

C. MODEL AT THE DC SIDE OF THE NPC

The inverter has two capacitors (C_p, and C_n) at the DC side, but to simplify the model both capacitors will have the same value (C). Using the current Kirchhoff law, the currents i_{cp}

TABLE 1. BPV array parameters.

Parameter	Value
N_s	1800u
N_p	200 u.
S_o	1000 W/m^2
R_s	0.008 Ω
R_{sh}	1000 Ω
I_{sco}	3.8 A
I_o	2.16e-8 A
n	1.2 p.u.

and i_{cn} on each capacitor are given by:

$$i_{cp}(t) = C_p \frac{d}{dt} v_p(t) = i_{dc}(t) - i_p(t)$$

$$i_{cn}(t) = C_n \frac{d}{dt} v_n(t) = i_{dc}(t) - i_n(t) \quad (6)$$

The top and bottom currents (i_p and i_n) on the DC side of the NPC depend upon the state of the switches of each leg upon the output currents (i^a, i^b, & i^c), as:

$$i_p(t) = S_{a1}(t)i^a(t) + S_{b1}(t)i^b(t) + S_{c1}(t)i^c(t),$$

$$i_n(t) = S_{a2}(t)i^a(t) + S_{b2}(t)i^b(t) + S_{c2}(t)i^c(t). \quad (7)$$

Furthermore, applying the voltage Kirchhoff law in the BPV array:

$$v_{dc}(t) = v_p(t) + v_n(t). \quad (8)$$

D. BPV ARRAY MODEL

The BPV array in FIGURE 1 is based on N_s series and N_p parallel strings connection of BPV cells. Each cell is modeled using the Single Diode Model [19], whose equivalent electric circuit is shown in FIGURE 3. The arrangement in this work is capable of generating 600kW operating under Standard Test Conditions, i.e., irradiance $S_0 = 1000$ W/m^2, temperature $T_0 = 25\,°C$ and the Air Mass $AM = 1.5$. Assuming equal cells operating in equal environmental conditions, the power generated by the entire array, at a certain given time, can be calculated with the following equations:

$$P_{pv} = i_{pv}v_{dc} = f(T, S, v_{dc}), \quad (9)$$

$$i_{pv} = I_{sco}\frac{S}{S_o}N_p - I_oN_p \left(e^{\left(\frac{v_d^T/N_s}{nkT}q\right)} - 1 \right) - \frac{v_d^T/N_s}{R_{sh}N_p}, \quad (10)$$

where,

$$v_d^T = v_{dc} + \frac{N_sR_si_{pv}}{N_p}. \quad (11)$$

The cell parameters are the rated short-circuit current (I_{sco}), the reverse saturation current of the diode (I_o), series resistance (R_s), parallel resistance (R_{sh}), ideality factor (n) and the electron charge and Planck's constant, q and k respectively. Table 1 summarizes the parameters of a typical cell. Clearly, i_{pv} depends directly on the irradiance (S) and on the temperature (T) to which the cells operate.

III. DC LINK CONTROL

The BPV solar array is connected directly to the NPC inverter, and to follow the maximum power point, the MPPT algorithm of [7] is implemented. This algorithm is based on measuring cells that together with the cell model estimate the M_{PP} voltage which is set to be the DC-link voltage reference. A PI controller is designed for the DC-link voltage, where the dynamic of the capacitors can be defined as:

$$h_{C_{dc}}(s) = -4/Cs, \quad (12)$$

by the procedure shown in [12]. Considering the model in (12), and a PI controller, $h_c^{dc}(s) = k_c(1 + 1/(T_is))$, the closed loop transfer function becomes:

$$h_{CL}(s) = \frac{\frac{-4}{C}\frac{k_c}{T_i}(T_is + 1)}{s^2 + \frac{-4}{C}k_cs + \frac{-4}{C}\frac{k_c}{T_i}}. \quad (13)$$

Now, by matching the desired characteristically polynomial $p_c(s) = s^2 + 2\xi\omega_ns + \omega_n^2$, with the characteristic polynomial in (13), the parameters results to be:

$$k_c = -\frac{\xi\omega_nC}{2}, \quad T_i = \frac{2\xi C}{\omega_n}. \quad (14)$$

The sample time (T_s), proportional gain (k_c) and integrative time (T_i) parameters of the PI controller are shown in Table 2. The i^q reference is set to zero to obtain a unitary displacement power factor at the grid, the i^d reference is set by the control of v_{dc} (see FIGURE 1). The $\alpha\beta$ current references based on the dq components are obtained using the transformation:

$$i_{ref}^\alpha(t) = \sin(\omega_st)i_{ref}^d(t), \quad i_{ref}^\beta(t) = -\cos(\omega_st)i_{ref}^d(t) \quad (15)$$

The complete control scheme is shown in FIGURE 1.

IV. PREDICTIVE CURRENT CONTROL

To track the current references in (15), a MPC is used. The MPC is one of the most popular approach to control power converters. This control technique is based on the inverter model, defined, in this case, in (1) to (8). Those equations can be discretized by the Euler-forward approximation, where $dx/dt = (x(k+1) - x(k))/T_s$.

The active and reactive power control is performed through the currents, therefore, the currents need to follow the references to achieve what is desired. In the case of the current prediction, based on (2), it is defined as:

$$\hat{\mathbf{i}}^{\alpha\beta}(k+1) = \mathbf{i}^{\alpha\beta}(k)\left(1 - \frac{T_sR}{L}\right) + \frac{T_s}{L}\left(\mathbf{v}^{\alpha\beta}(k) - \mathbf{v}_s^{\alpha\beta}(k)\right), \quad (16)$$

where $\hat{\mathbf{i}}^{\alpha\beta}(k+1)$ represents the estimation of $\mathbf{i}^{\alpha\beta}(k+1)$. This method is used for both the traditional FS-MPC and the proposed FFS-MPC.
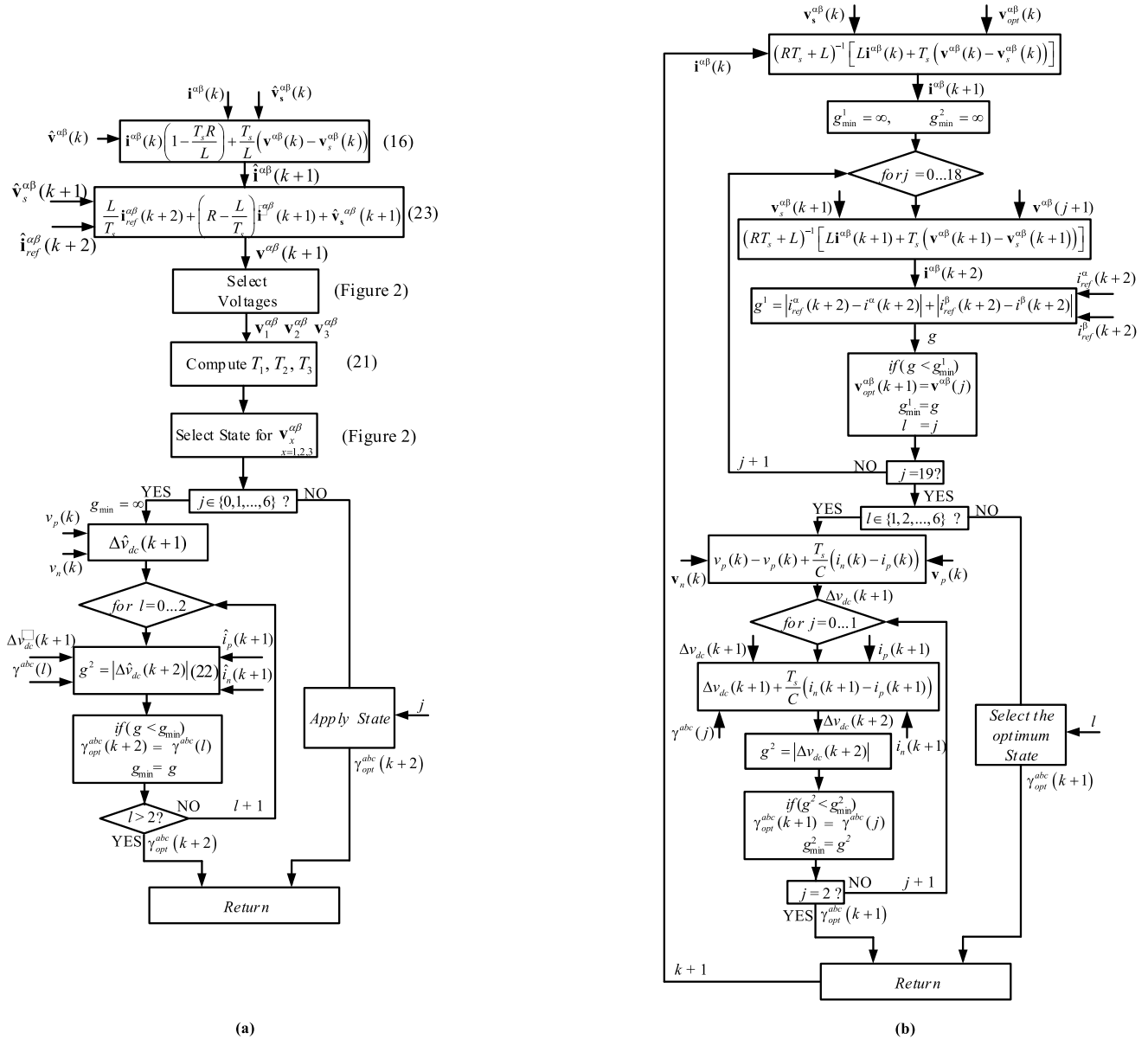
FIGURE 4. NPC predictive control algorithms (a) Proposed FFS-MPC (b) Traditional FS- MPC algorithm.

A. TRADITIONAL FS-MPC

In the traditional FS-MPC, all the possible states must be tested, using the model, and then, applying the state which minimizes a cost function. Furthermore, due to the computation delay, (16) must be forwarded one step ahead, [12].

Despite the NPC has 19 voltages, the short and zero voltages have more than one state, FIGURE 2 (a), resulting in 27 states. Those additional states are used to reduce the imbalance between the voltage v_p and v_n. The equations (6) to (8) are used together with the Euler approximation, with the following results:

$$v_p(k+1) \approx \hat{v}_p(k+1) = v_p(k) + \frac{T_s}{C_p}\left(i_{dc}(k) - i_p(k)\right)$$

$$v_n(k+1) \approx \hat{v}_n(k+1) = v_p(k) + \frac{T_s}{C_n}\left(i_{dc}(k) - i_n(k)\right) \quad (17)$$

The voltage deviation between v_p and v_n, assuming that $C_p = C_n = C$, becomes:

$$\Delta v_{dc}(k+1) \approx \Delta \hat{v}_{dc}(k+1) = \hat{v}_p(k+1) - \hat{v}_n(k+1)$$

$$\Delta \hat{v}_{dc}(k+1) = v_p(k) - v_n(k) + \frac{T_s}{C}\left(i_n(k) - i_p(k)\right) \quad (18)$$

As the calculated states are to be applied in the time $k+1$, the voltage difference in (18) need to be one step forwarded:

$$\Delta \hat{v}_{dc}(k+2) = \Delta \hat{v}_{dc}(k+1) + \frac{T_s}{C}\left(\hat{i}_n(k+1) - \hat{i}_p(k+1)\right). \quad (19)$$

The simplest FS-MPC algorithm defines a cost function as:

$$g^3 = k_1 \left| i_{ref}^\alpha(k+2) - \hat{i}^\alpha(k+2) \right|$$

$$+ k_2 \left| i_{ref}^\beta(k+2) - \hat{i}^\beta(k+2) \right| + k_3 \left| \Delta \hat{v}_{dc}(k+2) \right| \quad (20)$$
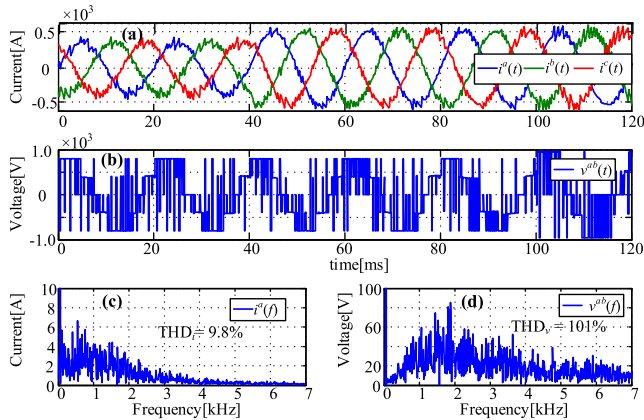
FIGURE 5. Key waveforms associated to the current control of Traditional FS-MPC; (a) $i^{abc}(t)$. (b) $v^{ab}(t)$, (c) $i^a(f)$, (d) $v^{ab}(f)$.

which guarantees the tracking of the current reference and, at the same time, reduces the voltage difference between v_p and v_n. Thus, as there are 27 valid states, the algorithm needs to compute the model 27 times to choose the best one to minimize g^3.

One improvement on this algorithm is to choose the best voltage (instead of the best state), among the 19 possible voltages, and go to a second loop only if there is chosen a short or zero voltage (which have more than one state), leading to include at most 22 iterations to find the best state. Thus, two cost functions are defined:

$$g^1 = \left| i_{ref}^{\alpha}(k+2) - \hat{i}^{\alpha}(k+2) \right| + \left| i_{ref}^{\beta}(k+2) - \hat{i}^{\beta}(k+2) \right| \tag{21}$$

for the first loop (voltage selection) and

$$g^2 = \left| \Delta\hat{v}_{dc}(k+2) \right| \tag{22}$$

for the second loop (state selection). The entire FS-MPC algorithm is shown in FIGURE 4 (b).

B. PROPOSED FFS-MPC

The proposed FFS-MPC also uses (16), but instead of trying all the valid states, it defines directly the voltage to be applied in the next step as:

$$\mathbf{v}^{\alpha\beta}(k+1) = \frac{L}{T_s}\mathbf{i}_{ref}^{\alpha\beta}(k+2) + \left(R - \frac{L}{T_s}\right)\hat{\mathbf{i}}^{\alpha\beta}(k+1)$$
$$+ \hat{\mathbf{v}}_s^{\alpha\beta}(k+1). \tag{23}$$

where $\mathbf{i}_{ref}^{\alpha\beta}(k+2)$ is set as the reference, $\mathbf{i}_{ref}^{\alpha\beta}(k+1)$ is found from (16) and $\hat{\mathbf{v}}_s^{\alpha\beta}(k+1)$ can be estimated by the Lagrange extrapolation [18], [21].

To impose the voltage $\mathbf{v}^{\alpha\beta}(k+1)$, it is synthetized by SVM modulation technique, which guarantees a fixed switching spectrum. In other words, the voltage in (23) is obtained by using a combination in time of the three nearest voltages, see FIGURE 2 (a) and (b):

$$T_s\hat{\mathbf{v}}^{\alpha\beta} = T_1\mathbf{v}_1^{\alpha\beta} + T_2\mathbf{v}_2^{\alpha\beta} + T_3\mathbf{v}_3^{\alpha\beta}$$
$$T_1 + T_2 + T_3 = T_s \tag{24}$$

TABLE 2. System parameters.

Parameter	Value
T_s	1 ms
k_c	-1.7 p.u.
T_i	0.01 p.u.
L	1 mH
C	9.4 mF
R	0.5 Ω
f_s	50 Hz
v_s^{aN}	220 V_{rms}
f_{sw}	3 kHz

TABLE 3. Operations for every algorithm.

Algorithm	Operation	Number of operations	Time to evaluate
	First loop (with 19 steps)		
	Sums	10	26.7 ns×10×19
	Subtractions	11	33.4 ns×11×19
	Multiplications Divisions	20	60.0 ns×20×19
Traditional Algorithm FS-MPC	*For, if, and other instructions*	10	26.7 ns×10×19
	Second Loop (with 2 steps)		
	Sums	10	26.7 ns×10×2
	Subtractions	11	33.4 ns×11×2
	Multiplications Divisions	20	60.0 ns×20×2
	For, if, and other instructions	8	26.7 ns×8×2
	Total Time		**44.03 µs**
	Proposed Algorithm		
	Sums	19	26.7 ns×19×1
	Subtractions	45	33.4 ns×45×1
	Multiplications	51	60.0 ns×51×1
Proposed Algorithm FFS-MPC	*Divisions*	3	220 ns×3×1
	For, if, and other instructions	13	26.7 ns×13×1
	acos(·)	1	410 ns×1×1
	Magnitude	1	280 ns×1×1
	Total Time		**6.72 µs**

Now, if, at least, one or more of the three nearest voltage are the short and/or zero voltage, a second loop is implemented to minimize the voltage difference, applying the same g^2 as in (22). The proposed FFS-MPC algorithm is illustrated in FIGURE 4 (a).

V. COMPUTATIONAL EFFORT AND COMPARISON WITH FS-MPC

The FFS-MPC obtains the converter voltage to be applied directly, where this voltage is synthetized by SVM technique. Once the converter voltage is decided, if and only if there exist redundancy, the DC link voltage balancing subroutine takes place by choosing the one that minimize this difference.

If the FFS-MPC algorithm is compared with the traditional FS-MPC, shown in FIGURE 4 (b), the computational cost is notably reduced, because FS-MPC tries all the possible states choosing the one that minimizes the cost functional and therefore it needs to evaluate the complete model several
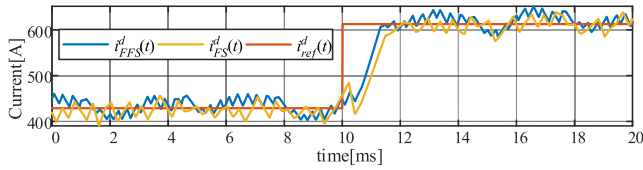
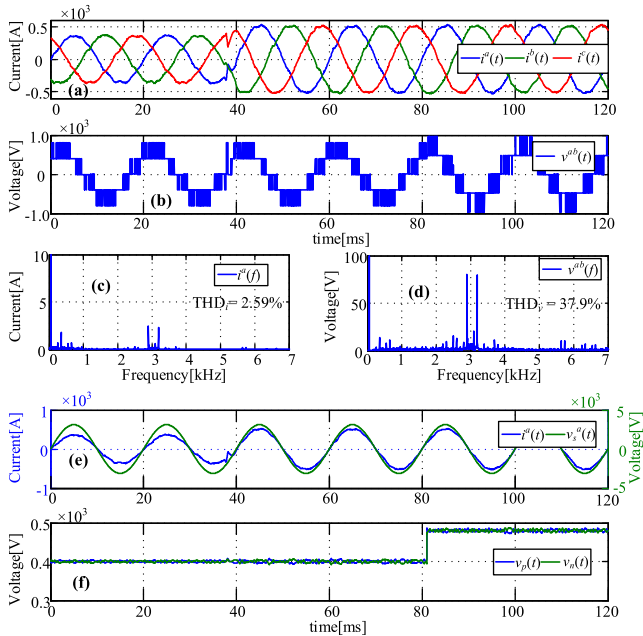**FIGURE 6.** Comparison in the time response between the proposed FFS-MPC and the traditional FS-MPC.

FIGURE 7. Key waveforms associated to the current control; (a) $i^{abc}(t)$. (b) $v^{ab}(t)$, (c) $i^a(f)$, (d) $v^{ab}(f)$, (e) $v_s^a(t)$ and $i^a(t)$, (f) $v_p(t)$ and $v_n(t)$.

FIGURE 8. AC Current. (a) Step change in the AC currents: top $i^a(t)$, $v_s^a(t)$, bottom $v^{ab}(t)$. (b) $i^a(f)$ in steady state.

FIGURE 9. DC link voltage step up; (a) top: Current and Voltage of phase a, $i^a(t)$, $v_s^a(t)$, Bottom: injected AC voltage, $v^{ab}(t)$, (b) DC link capacitors voltages, $v_p(t)$ and $v_n(t)$.

times, more details of this algorithm can be found in [12], [17], [18]. In contrast, the proposed algorithm, shown in FIGURE 4 (a), sets the voltage to be applied directly. In fact, VI-A shows the total amount of operations that requires both algorithms, giving a fair comparison to evaluate the computation requirements.

The VI-A shows the operations needed to implement the FS-MPC and the FFS-MPC, where the acquisition, the PLL, the Clark Transformation and the states writing times, are not considered as these stages are the same for both algorithms. Just to give an example, the fourth column of VI-A depicts the computing time for every operation considering the TMS320F28335 DSP based board [20] to highlight the difference in the total computing time. As it can be seen, the FS-MPC takes about 44 μs to execute the code, and the FFS-MPC takes around 7 μs, being the FS-MPC at least 6 times heavier than the FFS-MPC. This allows to implement the proposal algorithm in a greater variety of digital boards, reducing the cost related to the controller.

Additionally, the FFS-MPC control has a better frequency spectrum. FS-MPC has a typical spread out spectrum, as can be seen in FIGURE 5. However, the proposed FFS-MPC shows a lower THD and a more concentrated spectrum that also allows an easier filter design, FIGURE 7.
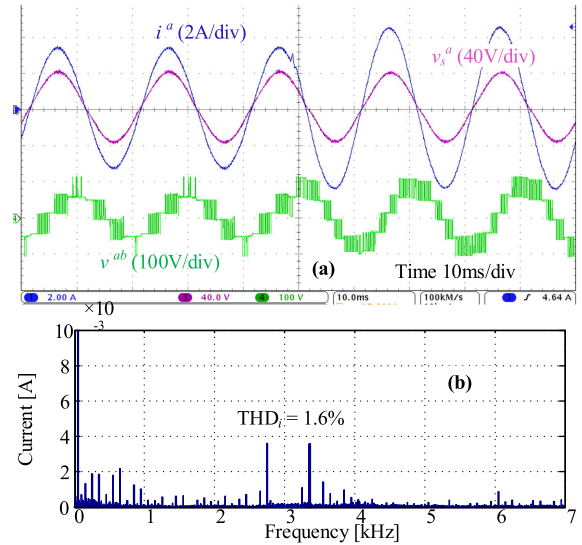
To compare the time response, two simulations are performed to notice the current control bandwidth, which can be seen in FIGURE 6. This figure shows a similar response, the proposed FFS-MPC is even a quietly faster from this comparison, and therefore the computational reduction does not affect in the dynamic performance.

VI. RESULTS
A. SIMULATED RESULTS
The parameters of the simulations are shown in Table 2 and were performed in PSim. To validate the proposed FFS-
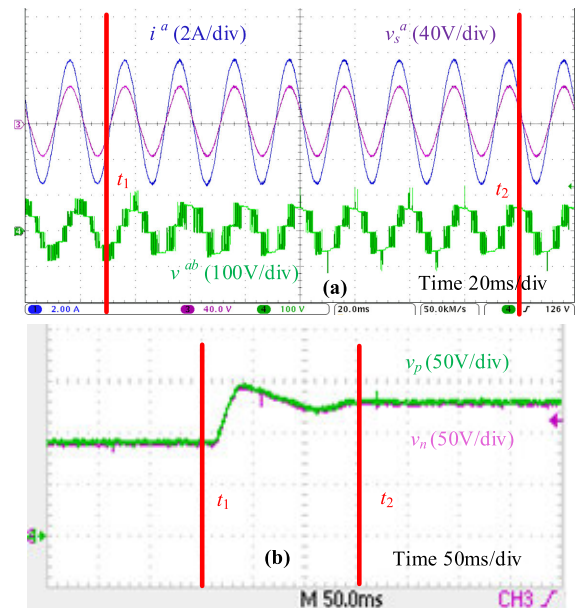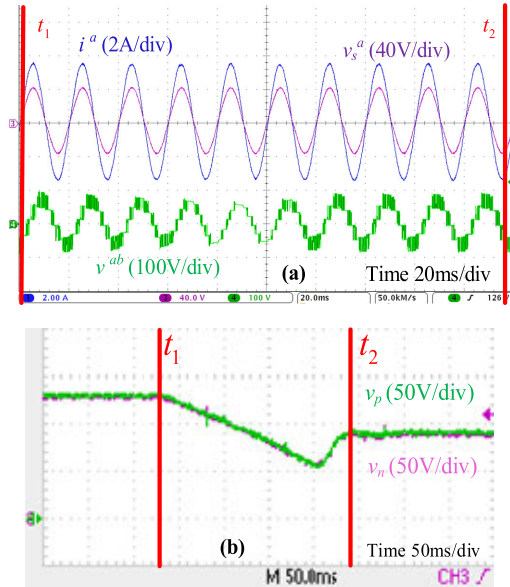
FIGURE 10. DC link voltage step down; (a) top: Current and Voltage of phase a, $i^a(t)$, $v_s^a(t)$, Bottom: injected AC voltage, $v^{ab}(t)$, (b) DC link capacitors voltages, $v_p(t)$ and $v_n(t)$.

TABLE 4. Experimental parameters.

Parameter	Value
R	10 Ω
L	15 mH
C	4.7 mF
f_{sw}	3 kHz
f_s	50 Hz

MPC current control, the key waveforms of the simulation of the photovoltaic system are presented in FIGURE 7. At the instant of time $t = 98$ms a change is made in the current reference, which can be seen in FIGURE 7 (a) and FIGURE 7 (c). At $t = 142$ms, the DC voltage source increases by 20%, which can be seen in FIGURE 7 (b) and FIGURE 7 (d), it can also be seen that the proposed control strategy is capable of maintaining the voltages balanced on the capacitors. In FIGURE 7 (c) it is seen that the system operates in perfect synchrony with the network voltage and using the changes imposed, it operates with unitary power factor. Finally, FIGURE 7 (e) and FIGURE 7 (f) show the harmonic content of the current i^a and voltage v^{ab} of the converter respectively, operating in steady state, it can be seen that the switching frequency is fixed and around 3 kHz.

B. EXPERIMENTAL RESULTS

The experimental results are obtained using a *RL* filter, a PV electronic emulator and a programmable three-phase source. The used parameters are given in Table 4 and the topology of FIGURE 1.

1) CURRENT CONTROL TEST: STEP CHANGES

In FIGURE 8 the key waveforms due to a step change in the current references keeping constant the DC voltage are shown. The AC voltage gets adapted in less than 2 ms in order to track the AC current references. The DC link
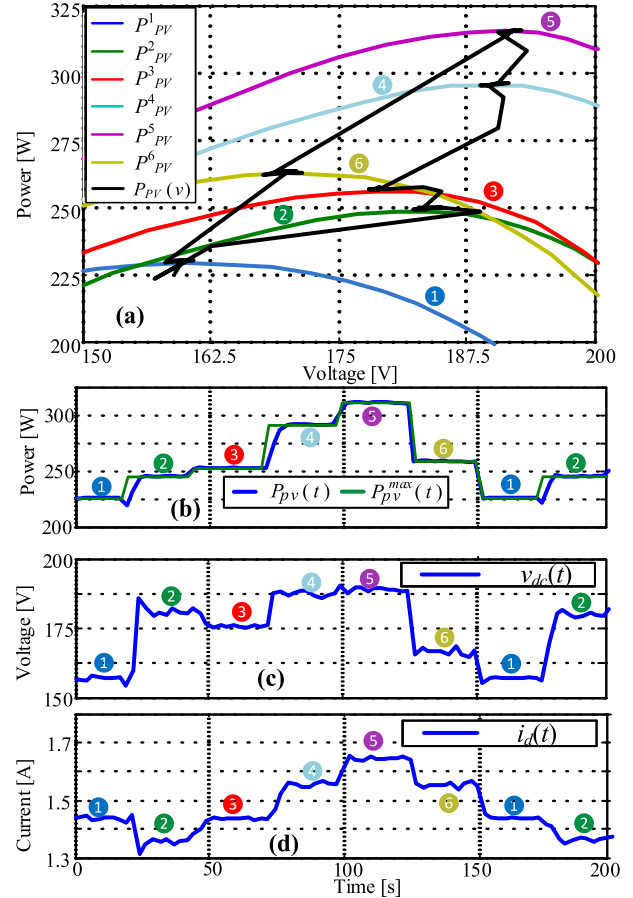

FIGURE 11. BPV emulator profiles sequential test; (a) power / voltage profiles ($P_{pv}(v)$), (b) instantaneous power ($P_{pv}(t)$), (c) DC link voltage ($v_{dc}(t)$), (d) BPV current ($i_{dc}(t)$).

voltage balance can be observed in the symmetric AC voltage waveforms (v^{ab}).

The DC link voltage increases from 180 V to 260 V, FIGURE 9, and the AC currents remain unchanged while the overall DC link voltage increases, FIGURE 9 (a), and the DC link voltages remain balanced, FIGURE 9 (b).

The DC link voltage is reduced from 260 V to 180 V, FIGURE 10. The AC current remains despite the under voltage of the DC link voltage that produces a saturated AC voltage, FIGURE 10 (a), in spite of everything, the DC link voltages remain balanced, FIGURE 10 (b).

2) CURRENT CONTROL TEST: FREQUENCY CHANGES

FIGURE 12 shows a frequency step change from 45 Hz to 60 Hz, where the current control maintains the power factor after this step, and the DC voltage is not affected, as it can be seen in the v^{ab} injected voltage. The current dynamic is fast, taking less than two cycles to return to unitary power factor.

3) COMPLETE LOOP TEST: TEMPERATURE AND RADIATION CHANGES

The DC voltage is provided by a PV electronic emulator (Magna Power SL600-4.3) that is programmed with 6 dif-
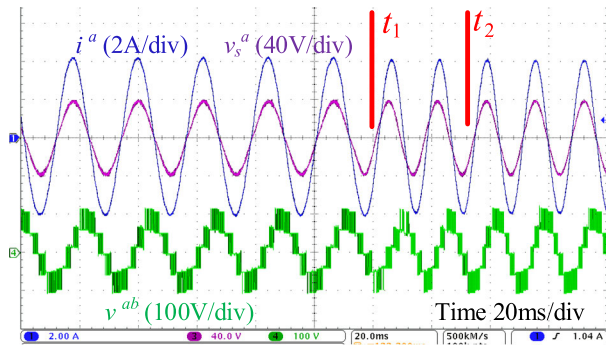
FIGURE 12. Grid frequency change; top: AC currents, bottom: AC voltage.

ferent BPV profiles (P_{PV}^1, P_{PV}^2,..., P_{PV}^6), using the PPPE software, FIGURE 12. These different profiles emulate different environmental conditions *i.e.* changes of irradiation and temperature. A loop is programmed so that every 25 s the P_{PV} profiles change sequentially in an infinite loop, FIGURE 11. The inverter uses an MPPT algorithm to establish the DC voltage reference to guarantee maximum power generation, which is tracked, FIGURE 11 (c), and it can be seen how the system is able to reach the maximum power points, FIGURE 11 (a) and (b).

Key waveforms are shown in FIGURE 11. The DC link voltage, FIGURE 11 (c), changes every 10 s in order to cover sequentially the six profiles and FIGURE 11 (a) shows the correct DC link voltage setting as the maximum DC power generation is achieved in each profile.

VII. CONCLUSION
The proposed FFS-MPC has the ability to inject power from a photovoltaic source, with good performance and, specially, with reduced computational effort and concentrated spectrum. In fact, it does not have a main cost function unlike the typical predictive controls that evaluates a complex cost function up to 27 times, also it does not calculate the imbalance on the future voltage of the capacitors in each possible state, indeed, it only does so in the low voltages to apply up to three times, reducing in 84% the computational effort. On the other hand, the harmonic content of the switching is less dispersed than in the typical predictive control. A laboratory scale plant was built, and the results are in whole agreement with the simulations. In fact, the maximum power point in BPV plant is reached, and the voltage imbalance in the capacitors is zero for all practical purposes. One limitation of this approach is the need of PWM modules to synthetize the SVM technique, because the SVM is timing sensitive. On the other hand, this approach can be extended to micro-grids, where the grid frequency and voltage amplitude may suffer disturbances in the values. Additionally, the aforementioned MPC method can be extended to the voltage control as well, since it can be modeled and therefore a similar technique is possible to be applied.

REFERENCES
[1] A. Qazi, F. Hussain, N. A. Rahim, G. Hardaker, D. Alghazzawi, K. Shaban, and K. Haruna, "Towards sustainable energy: A systematic review of renewable energy sources, technologies, and public opinions," *IEEE Access*, vol. 7, pp. 63837–63851, 2019.

[2] F. Wang, Z. Li, X. Tong, and L. Chen, "Modeling, analysis and evaluation of modified model predictive control method for parallel three-level simplified neutral point clamped inverters," *IEEE Access*, vol. 7, pp. 185349–185359, 2019.

[3] N. Kumar, I. Hussain, B. Singh, and B. K. Panigrahi, "Framework of maximum power extraction from solar PV panel using self predictive perturb and observe algorithm," *IEEE Trans. Sustain. Energy*, vol. 9, no. 2, pp. 895–903, Apr. 2018.

[4] N. E. Zakzouk, B. W. Williams, A. A. Helal, M. A. Elsaharty, and A. K. Abdelsalam, "Improved performance low-cost incremental conductance PV MPPT technique," *IET Renew. Power Gener.*, vol. 10, no. 4, pp. 561–574, Apr. 2016.

[5] J. Silva, J. Espinoza, J. Rohten, M. Torres, and E. Espinosa, "Grid connected PV system with maximum power point estimation based on reference cells," in *Proc. IECON-41st Annu. Conf. IEEE Ind. Electron. Soc.*, Yokohama, Japan, Nov. 2015, pp. 004070–004075.

[6] D. Ickilli, H. Can, and K. S. Parlak, "Development of a FPGA-based photovoltaic panel emulator based on a DC/DC converter," in *Proc. 38th IEEE Photovoltaic Specialists Conf.*, Austin, TX, USA, Jun. 2012, pp. 1417–1421.

[7] R. Morales, M. Garbarino, J. Munoz, C. Baier, J. Rohten, V. Esparza, and D. Dewar, "Grid connected PV system with new MPPT estimation method based on measuring cells," in *Proc. IECON-45th Annu. Conf. IEEE Ind. Electron. Soc.*, Lisbon, Portugal, Oct. 2019, pp. 2366–2371.

[8] A. Asgharzadeh, B. Marion, C. Deline, C. Hansen, J. S. Stein, and F. Toor, "A sensitivity study of the impact of installation parameters and system configuration on the performance of bifacial PV arrays," *IEEE J. Photovolt.*, vol. 8, no. 3, pp. 798–805, May 2018.

[9] J. E. Castillo-Aguilella and P. S. Hauser, "Multi-variable bifacial photovoltaic module test results and best-fit annual bifacial energy yield model," *IEEE Access*, vol. 4, pp. 498–506, 2016.

[10] X. Sun, M. R. Khan, C. Deline, and M. A. Alam, "Optimization and performance of bifacial solar modules: A global perspective," *Appl. Energy*, vol. 212, pp. 1601–1610, Feb. 2018.

[11] H. Nademi, A. Das, R. Burgos, and L. E. Norum, "A new circuit performance of modular multilevel inverter suitable for photovoltaic conversion plants," *IEEE J. Emerg. Sel. Topics Power Electron.*, vol. 4, no. 2, pp. 393–404, Jun. 2016.

[12] J. A. Rohten, J. R. Espinoza, J. A. Munoz, D. G. Sbarbaro, M. A. Perez, P. E. Melin, J. J. Silva, and E. E. Espinosa, "Enhanced predictive control for a wide time-variant frequency environment," *IEEE Trans. Ind. Electron.*, vol. 63, no. 9, pp. 5827–5837, Sep. 2016.

[13] S. Mukherjee, S. Kumar Giri, S. Kundu, and S. Banerjee, "A generalized discontinuous PWM scheme for three-level NPC traction inverter with minimum switching loss for electric vehicles," *IEEE Trans. Ind. Appl.*, vol. 55, no. 1, pp. 516–528, Jan./Feb. 2019.

[14] L. Zheng, F. Jiang, J. Song, Y. Gao, and M. Tian, "A discrete-time repetitive sliding mode control for voltage source inverters," *IEEE J. Emerg. Sel. Topics Power Electron.*, vol. 6, no. 3, pp. 1553–1566, Sep. 2018.

[15] J. R. Espinoza and G. Joos, "State variable decoupling and power flow control in PWM current-source rectifiers," *IEEE Trans. Ind. Electron.*, vol. 45, no. 1, pp. 78–87, Feb. 1998.

[16] L. Tarisciotti, A. Formentini, A. Gaeta, M. Degano, P. Zanchetta, R. Rabbeni, and M. Pucci, "Model predictive control for shunt active filters with fixed switching frequency," *IEEE Trans. Ind. Appl.*, vol. 53, no. 1, pp. 296–304, Jan./Feb. 2017.

[17] A. K. Bonala, S. R. Sandepudi, and V. P. Muddineni, "Selective finite-states model predictive control of grid interfaced three-level neutral point clamped photovoltaic inverter for inherent capacitor voltage balancing," *IET Power Electron.*, vol. 11, no. 13, pp. 2072–2080, Nov. 2018.

[18] J. Silva, J. Espinoza, D. Sbarbaro, L. Moran, J. Rohten, and L. Vaccaro, "Fast MPC algorithm for a grid tied photovoltaic system based on a multilevel inverter," in *Proc. IECON-45th Annu. Conf. IEEE Ind. Electron. Soc.*, Lisbon, Portugal, Oct. 2019, pp. 3989–3994.

[19] S. A. Pelaez, C. Deline, P. Greenberg, J. S. Stein, and R. K. Kostuk, "Model and validation of single-axis tracking with bifacial PV," *IEEE J. Photovolt.*, vol. 9, no. 3, pp. 715–721, May 2019.

[20] M. P. Kazmierkowski, M. Jasinski, and G. Wrona, "DSP-based control of grid-connected power converters operating under grid distortions," *IEEE Trans. Ind. Informat.*, vol. 7, no. 2, pp. 204–211, May 2011.

[21] M. Rivera, S. Kouro, J. Rodriguez, B. Wu, V. Yaramasu, J. Espinoza, and P. Melila, "Predictive current control in a current source inverter operating with low switching frequency," in *Proc. 4th Int. Conf. Power Eng., Energy Electr. Drives*, Istanbul, Turkey, May 2013, pp. 334–339.

ESTEBAN S. PULIDO (Student Member, IEEE) received the B.S. and M.Sc. degrees in electrical engineering from the Universidad Técnica Federico Santa María (UTFSM), Valparaíso, Chile, in 2002 and 2006, respectively. He is currently pursuing the Ph.D. degree in electrical engineering with the University of Concepción, Concepción, Chile.

He was a Power System Analyst and an Engineer Operation and Planning at Transelec Transmission Company, Santiago, Chile, from 2006 to 2012. Since 2013, he has been an Assistant Professor with the Department of Electrical Engineering, UTFSM. His main research interests include the power protection systems, power systems transients, and the integration of renewable energy systems.

JOSE J. SILVA (Member, IEEE) received the Engineering degree (Hons.) in electronic engineering and the M.Sc. degree in electrical engineering from the University of Concepción, Concepción, Chile, in 2014 and 2015, respectively. Since 2015, he has been teaching in the area of control and electrical. He is conducting Ph.D. research in the area of photovoltaic systems operating under partial shading conditions. In addition, his research interests include weak grids, wind systems, digital control, multilevel converters, and model predictive control, among others.

FELIPE A. VILLARROEL received the B.Sc. and Engineer degrees (Hons.) in electronic engineering and the M.Sc. degree in electrical engineering from the University of Concepción, Concepción, Chile, in 2007, 2009, and 2012, respectively. where he is currently pursuing the Ph.D. degree in electrical engineering, sponsored by a scholarship from the Chilean Research Foundation CONICYT. Since late 2012 until February 2016, he worked as a Hardware/Software Engineer at CADETECH S.A., Concepción. His research interests include the modeling, simulation, and control of power converters, in particular predictive control techniques.

JOSE R. ESPINOZA (Senior Member, IEEE) received the Engineering degree in electronic engineering and the M.Sc. degree in electrical engineering from the University of Concepción, Concepción, Chile, in 1989 and 1992, respectively, and the Ph.D. degree in electrical engineering from Concordia University, Montreal, QC, Canada, in 1997. Since 2006, he has been a Professor with the Department of Electrical Engineering, University of Concepción, where he is engaged in teaching and research in the areas of automatic control and power electronics. He has authored and coauthored more than 150 refereed journals and conference papers and contributed to one chapter in the Power Electronics Handbook published in 2011 by Academic Press. He is currently an Associate Editor of the IEEE Transactions on Power Electronics and the IEEE Transactions on Industrial Informatics.

MIGUEL A. TORRES (Member, IEEE) received the M.Sc. degree in electrical engineering from the Universidad de Concepción, Chile, and the Ph.D. degree in electrical engineering from Concordia University, Montreal, QC, Canada, in 2013. In 2003, he was with l'École Supérieure d'Électricité, Paris, France, working on passivity-based control of voltage source converters. From 2005 to 2008, he worked in the industry as an Automation Engineer. His Ph.D. dissertation titled Dynamic Frequency Control in Diesel-Hybrid Autonomous Power Systems using Virtual Synchronous Machines. In July 2013, he joined the Chilean Solar Energy Research Center (SERC Chile) as a Postdoctoral Fellow, where he worked on the control of multicell converter topologies for the integration of large-scale photovoltaic plants into the grid. Since March 2017, he has been an Assistant Professor with the Institute of Engineering Sciences, Universidad de O'Higgins, Chile. In 2018, he rejoined SERC-Chile as an Invited Researcher. Since 2008, he has been working on virtual synchronous machines and its applications to the integration of renewable energies and grid stabilization. In 2017, he has coauthored a chapter in the fourth edition of the Power Electronics Handbook by M. Rashid. His research interests include control of power electronic converters, self-tuning virtual synchronous machines, and agro-PV systems.

JAIME A. ROHTEN (Member, IEEE) received the Engineering degree (Hons.) in electronic engineering and the M.Sc. and D.Sc. degrees in electrical engineering from the University of Concepción, Concepción, Chile, in 2010, 2012, and 2017, respectively. Since 2015, he has been teaching in the areas of power electronic and control systems analysis with the Department of Electrical and Electronic Engineering, Universidad del Bío-Bío, Concepción, Chile. His research interests include renewable energies, digital nonlinear, resonant, and predictive control for voltage or current source converters.

MAURICIO A. REYES was born in Concepción, Chile, in 1988. He received the B.Sc. and M.Sc. degrees in electrical engineering from the University of Concepción, in 2014 and 2020, respectively. His research interests include power electronics, control of power electronics, energy conversion, and renewable energies.

• • •